PCCP

PAPER

View Article Online
View Journal | View Issue

HPSTAR 163-2016

Pressure-driven semiconducting-semimetallic transition in SnSe

Cite this: *Phys. Chem. Chem. Phys.*, 2016, **18**, 5012

Jiejuan Yan,[a] Feng Ke,[b] Cailong Liu,[a] Li Wang,[a] Qinglin Wang,[b] Junkai Zhang,[b] Guanghui Li,[a] Yonghao Han,*[a] Yanzhang Ma[bc] and Chunxiao Gao*[a]

Received 30th November 2015,
Accepted 19th January 2016

DOI: 10.1039/c5cp07377d

www.rsc.org/pccp

In this work, we report the pressure-dependent electrical transport and structural properties of SnSe. In our experiments an electronic transition from a semiconducting to semimetallic state was observed at 12.6 GPa, followed by an orthorhombic to monoclinic structural transition. Hall effect measurements indicate that both the carrier concentration and mobility vary abnormally accompanied by the semimetallic electronic transition. First-principles band structure calculations confirm the semiconducting-semimetallic transition, and reveal that the semimetallic character of SnSe can be attributed to the enhanced coupling of Sn-5s, Sn-5p, and Se-3p orbitals under compression that results in the broadening of energy bands and subsequently the closure of the band gap. The pressure modulated variations of electrical transport and structural properties may provide an approach to improving the thermoelectric properties of SnSe.

1. Introduction

Tin selenide (SnSe) is a typical example of layered IV–VI compounds. It is currently under extensive study due to a finite energy band gap of 0.9–1.05 eV, a large absorption coefficient,[1,2] and a high photovoltaic conversion efficiency.[3] These properties are desired for optimizing the performance of solar cells and photovoltaic cells,[3–5] and many other applications. Recently, it was found that SnSe exhibited attractive thermoelectric performance because of its intrinsically ultralow thermal conductivity and high enough electrical conductivity.[6] The basic parameters of characterizing the performance of thermoelectric converters are the dimensionless figure of merit ZT, defined as $ZT = S^2\sigma T/(\kappa_{ele} + \kappa_{lat})$, where S, σ, κ_{ele} and κ_{lat} are the Seebeck coefficient, electrical conductivity, electronic and lattice thermal conductivity, respectively. For decades, several approaches have been applied to optimize the thermoelectric performance of materials, such as improving the Seebeck coefficients by tuning the band structure,[7] enhancing the carrier mobility,[8] changing the temperature dependence from semiconductive-like to metallic-like by doping,[9] and decreasing the lattice thermal conductivity by nanostructuring.[10] The electronic structure and the microstructure play significant roles in the thermoelectric performance of materials.

High pressure has been shown to be a powerful factor in modulating the crystallographic and electronic structures, and subsequently changing the energy band gap of materials. Pioneering studies have illustrated that both the free carrier concentration and mobility can be tuned significantly in layered selenides,[11–13] which provides a possible route for modulating the transport properties of SnSe. However, to date, the structural and electronic properties of SnSe under compression have been less understood, limiting the optimization of the performance of SnSe-based devices. Under ambient conditions, SnSe crystallizes into the layered orthorhombic crystal structure with *Pnma* symmetry. This crystal structure consists of two-atom-thick sheets with each Sn atom covalently bonded with three Se neighbors, which are stacked together by weaker van der Waals-like coupling along the *a*-direction. Early X-ray diffraction indicated that this layered crystal structure remained stable up to 34 GPa.[14] However, first-principles calculations suggested that SnSe transformed from the orthorhombic (*Pnma*) structure to the orthorhombic (*Cmcm*) structure at ~7 GPa by evaluating the system enthalpy difference of these two crystal structures.[15] On the other hand, X-ray diffraction measurements showed that SnS, isostructural to SnSe, transformed from the orthorhombic to monoclinic structure under pressure.[16] Recently, Loa *et al.* proposed that the high-pressure phase of SnSe should be an orthorhombic structure with *Pbnm* symmetry.[17] It seems that the pressure induced structural transition of SnSe is undetermined. Previous quasiparticle GW calculations predicted that SnSe should be metallic in the high-pressure phases,[18] while experimental evidence for the metallic SnSe is still absent. Despite the fact that great efforts have been made in studying the electronic structure of SnSe under compression by

[a] *State Key Lab for Superhard Materials, Institute of Atomic and Molecular Physics, Jilin University, Changchun 130012, China. E-mail: cc060109@qq.com, hanyh@jlu.edu.cn*
[b] *Center for High Pressure Science and Technology Advanced Research, Shanghai 201203, China*
[c] *Department of Mechanical Engineering, Texas Tech University, Lubbock, TX79409, USA*

the theoretical calculations[15,18] and resistance measurements in a low pressure range,[19–21] it remains unexplored how compression tunes the electrical transport parameters related to thermoelectric performance, including electrical resistivity (ρ), carrier concentration (n) and mobility (μ).

Motivated by the above mentioned issues, we evaluated the temperature dependence of electrical resistivity measurements to explore the high-pressure metallic behavior of SnSe. Hall effect measurements were also made to study the variation of carrier concentration and mobility under compression. Meanwhile, the structural properties of SnSe were monitored by using X-ray diffraction (XRD) measurements. TEM images of quenched samples were obtained to study the effect of compression on the microstructure of SnSe. First-principles calculations were performed to rationalize the pressure-induced variations of the electrical transport properties of SnSe. By combining these measurements, we found that SnSe became semimetallic above $\sim$12.6 GPa, followed by an orthorhombic to monoclinic structural transition, giving rise to the dramatic variations of the carrier concentration and mobility of SnSe. The average grain size of SnSe decreased significantly under compression.

2. Experimental section

The samples used for the electrical transport and XRD property measurements were powdered SnSe samples bought from Alfa Aesar Company, with a purity of 99.999%. High pressure was generated using a nonmagnetic diamond anvil cell (DAC) with an anvil culet of 300 μm in diameter. Four-probe Mo film microcircuits with the van der Pauw configuration were used for electrical transport property measurements. The fabrication of the Mo film microcircuits sputtered on diamond surfaces, the preparation of insulating gaskets, and other relevant experimental details were reported previously.[22,23] Fig. 1(a) and (b) illustrate the model of the film microcircuits and the schematic view of the experimental set-up. The thickness of the sample was determined using a micrometer with a precision of 0.5 μm, and the deformation of the diamond anvil was also taken into account.[24] Pressure was calibrated with the R_1 fluorescence peak of ruby.[25] The maximum magnetic field on Hall effect measurements of SnSe was 1.5 T applied parallel to the DAC. The current reversal method was used in electrical transport property measurements to avoid systematic errors resulting from the misalignment of probing electrodes and thermoelectric offset voltages. To avoid impurities and ensure good electrode contact, no pressure transmitting medium was used for the electrical transport measurements.

First-principles calculations were carried out using density functional theory within the GGA-PBE exchange-correlation[26] on the standard CASTEP program in the Material Studio package.[27] A kinetic cutoff energy of 500 eV, and appropriate Monkhorst-Pack k-point meshes ($3 \times 8 \times 8$ meshes) were set up for all structures to ensure the convergence of the enthalpy calculations.

In situ high-pressure XRD experiments were conducted at BL15U1 of Shanghai Synchrotron Radiation Facility (SSRF) and BL4W2 of Beijing Synchrotron Radiation Facility (BSRF) using the angle-dispersive XRD mode (λ = 0.6199 Å). The methanol–ethanol–water (16 : 3 : 1) mixture was used as the pressure transmitting medium in Run 1, and no pressure medium was used in Run 2 for better comparison of electrical transport properties. The experimental parameters including the distance between the sample and the detector were calibrated using the CeO_2 standard materials. The Bragg diffraction images were integrated using FIT2D software to obtain intensity *versus* diffraction angle 2θ patterns. XRD patterns were fitted using the GSAS program package.[28]

3. Results and discussion

Shown in Fig. 1(c) is the temperature dependence of electrical resistivity of pressurized SnSe in the temperature range of 80–270 K. At low pressures ($<$12.6 GPa), the temperature (T)-resistivity (ρ) curves exhibit a negative temperature dependence, $d\rho/dT < 0$, indicating the presence of a semiconducting state. For pressures of 12.6 GPa and above, a positive temperature dependence, $d\rho/dT > 0$, is observed at all temperatures, indicating the metallic or semimetallic character of SnSe (see Fig. 1d).

To gain a deeper insight into the carrier transport process behind the semiconducting-metallic transition, we performed *in situ* high-pressure Hall effect measurements. Fig. 2 shows the pressure dependence of electrical transport parameters (ρ, n, μ, and R_H) of SnSe measured at room temperature. At ambient pressure, the values of ρ, n, μ, and R_H are 0.02 Ω cm, 2.99×10^{19} cm^{-3}, 12.24 cm^2 V^{-1} s^{-1}and 0.21 cm^3 C^{-1}, respectively. The magnitude of resistivity and carrier mobility in our experiments is comparable with previous results.[6,29]

In the compression up to 12.2 GPa, ρ decreases dramatically with pressure by more than one order of magnitude (Fig. 2a). A pronounced variation is that ρ of SnSe changes its pressure dependence at $\sim$12.2 GPa and drops smoothly up to 25.0 GPa, the highest pressure in this measurement. During the decompression, the inflection pressure point of electrical resistivity re-emerges at $\sim$7.0 GPa. After being quenched to ambient pressure, the electrical resistivity of SnSe recovers to its original magnitude.

Shown in Fig. 2b and c is the pressure dependence of n and μ of SnSe. It can be found that, from ambient pressure to 12.2 GPa, n decreases with the increasing pressure, while μ improves by more than ten times. The increased carrier mobility can only be partially compensated by the decreased carrier concentration, which can be considered as the cause of dramatic reduction of electrical resistivity below 12.2 GPa. Based on the $k{\cdot}p$ model,[30] the effective mass of the free carrier should be decreased as the energy band-gap decreases, which may contribute to the increase in the carrier mobility of SnSe. Besides, the grain boundaries on powdered samples may also play a role in the changes of electrical transport parameters, especially in low pressure regions (below 5 GPa).[31,32] Upon further compression,

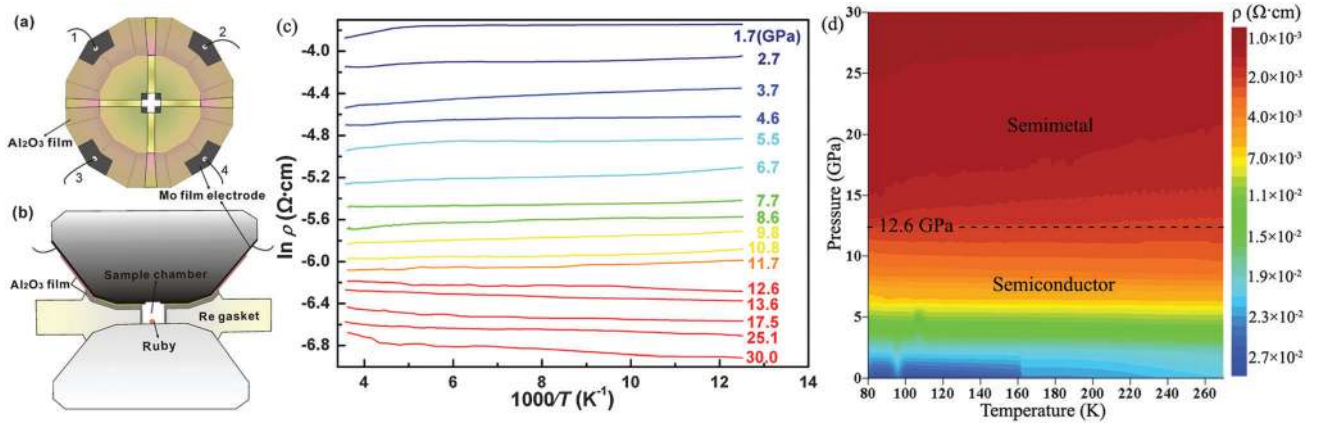

Fig. 1 (a) Configuration of Mo film microcircuits on diamond surfaces. (b) Cross-section of the designed DAC. (c) Temperature dependence of resistivity (ρ) of SnSe at various pressures. (d) Temperature-pressure contour plot of resistivity showing the transition region from the semiconductor to metallic or semimetallic region.

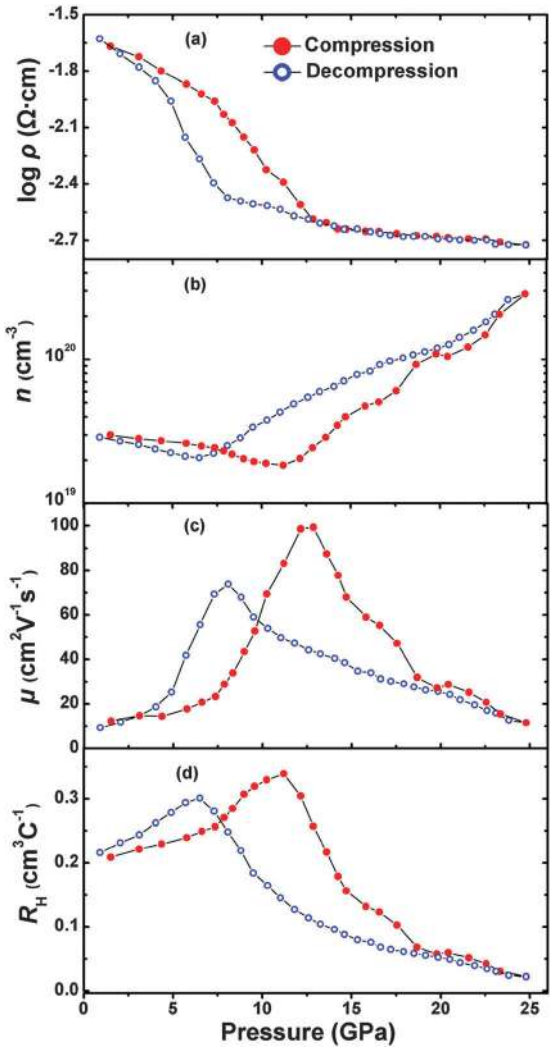

Fig. 2 Electrical resistivity (a), carrier concentration (b), carrier mobility (c), and hall coefficient (d) of SnSe as a function of pressure measured at room temperature. The experimental error is within 3%.

both n and μ of SnSe show abnormal variations at ~12.2 GPa. n inverts its pressure dependence and increases considerably up to 25.0 GPa. Meanwhile, μ goes through a sharp decrease above 12.2 GPa. Consequently, ρ of SnSe drops smoothly about 12.2 GPa. The increase of n can be attributed to the closure of the energy band gap. On the other hand, the free carrier scattering should be strengthened due to the increased carrier concentration.[33] Therefore, μ of SnSe drops significantly after the pressure-induced semiconducting to semimetallic transition. In the decompression process, both n and μ of SnSe change abnormally at ~7.0 GPa, and go back to their initial values when quenched to ambient conditions, showing reversible character as well. The different transition pressure in compression and decompression runs may be caused by the hysteresis effect.[34,35] The crystal structure requires enough time to recover completely to its initial state.

Shown in Fig. 2d is R_H of SnSe as a function of pressure. R_H remains positive from ambient pressure to 25.0 GPa, which clearly indicates that the hole carriers are more competitive than the electron carriers, and further implies that SnSe is semimetallic above 12.6 GPa.

The intriguing semiconductive-semimetallic transition of SnSe motivates us to explore the mechanisms behind. The discontinuous change of electrical transport properties usually coincides with crystal structural transition. XRD measurements were carried out to monitor the structural modification of SnSe under compression. Fig. 3(a) shows the selected XRD patterns of SnSe with methanol–ethanol–water (16 : 3 : 1) as the pressure transmitting medium. The XRD results with no pressure medium show similar observations (not shown in Fig. (3a)). At ambient pressure, the pattern of SnSe can be well indexed into the orthorhombic (*Pnma*) structure as in previously reported results.[36] It is found that, upon gradually increasing pressure up to 12.1 GPa, three new diffraction peaks at ~13.7°, ~14.3° and ~24.2° suddenly emerge, which clearly signals the I–II structural transition. Phase II remains stable up to 26.2 GPa, the highest pressure in this work. In the decompression, all the diffraction peaks of Phase I reappear and those of Phase II disappear,

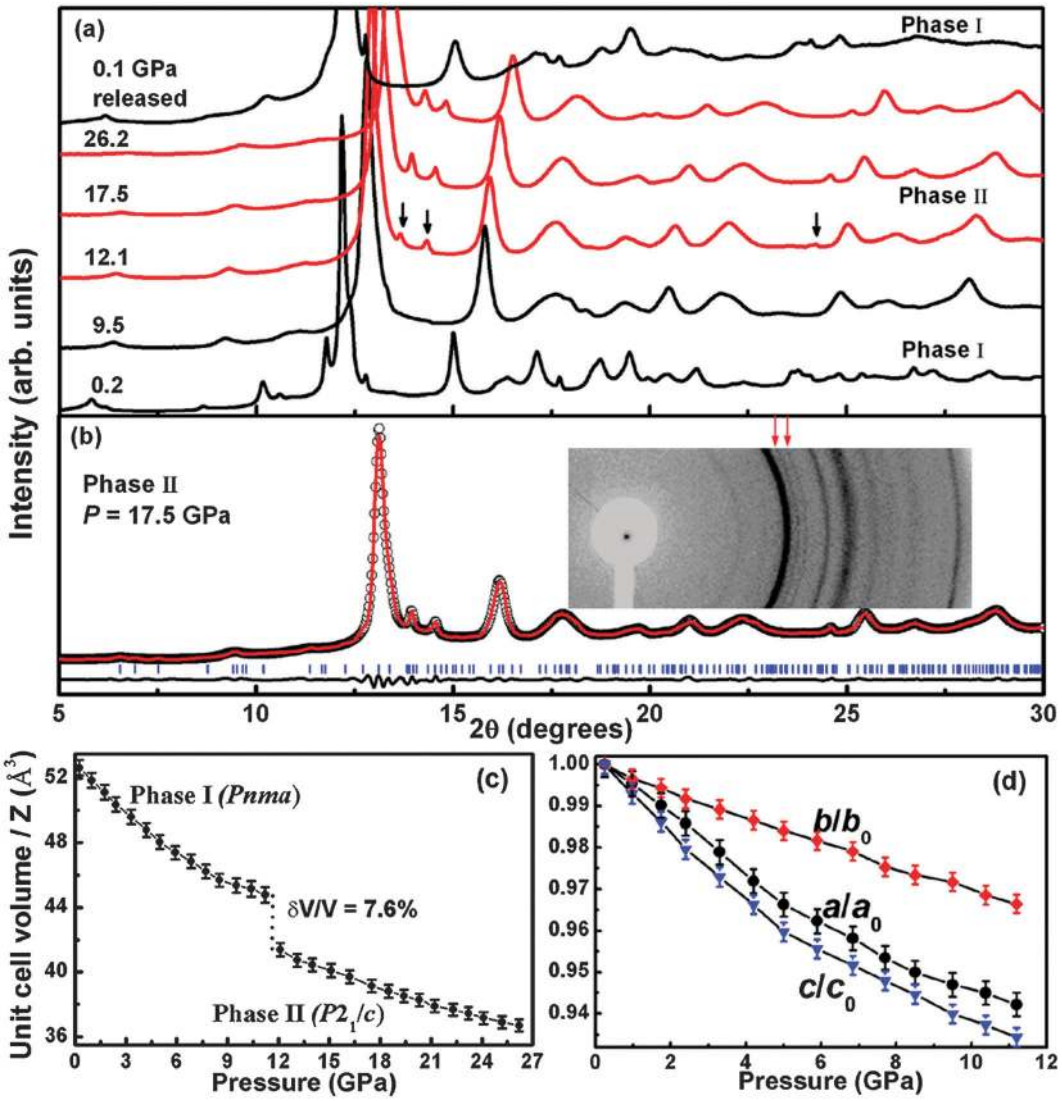

Fig. 3 (a) Representative XRD patterns of SnSe at various pressures with methanol–ethanol–water (16 : 3 : 1) as pressure transmitting medium. The XRD results with no pressure medium show similar observations (not shown). (b) The Li bail refinement results for Phase II at 17.5 GPa (R_w = 1.42% and R_{wp} = 3.13%). (c) Volume *versus* pressure data for phases I and II obtained using XRD and geometry optimization. (d) The lattice parameters as a function of pressure for Phase I.

indicating that the structural transition is reversible, consistent with our electrical transport property measurements. The patterns of Phase II can be indexed into the monoclinic structure. The previously reported structure with $P2_1/c$ symmetry on isostructural SnS[16] seems to match better with our experimental results. The lattice parameters of SnSe at 17.5 GPa are refined to a = 5.422 Å, b = 6.112 Å, and c = 9.469 Å, respectively. Unfortunately, the quality of the data beyond the structural transition was insufficient for further structural determination. We noticed that recently reported XRD measurements proposed that SnSe transformed to orthorhombic structures with *Pbnm* or *Cmcm* symmetries.[17,37] However, in our experiments, the diffraction peaks at ~13.7° and ~14.3° cannot be indexed into all of these structures. We infer that the different assigned structures may result from the low intensity of these two diffraction peaks in previous studies and hence were not indexed.[17,37] The structural transition is accompanied by a pronounced volume collapse of ~7.6%. The obtained bulk moduli (B_0) by fitting the P–V curves are 34.2 and 50.2 GPa with $B_0' = 4$.[17,37] The lattice compression of SnSe is found to be highly anisotropic. The compressibility along the c-axis is higher than those along a- and b-axes (Fig. 3d).

A previous study proposed that the nanostructuring approach was effective for reducing the thermal conductivity by enhancing the scattering of phonons due to the increased density of nanograin boundaries.[10] TEM images of quenched samples were obtained to study the variation of the microstructure of SnSe under compression. As shown in Fig. 4, the average grain size of SnSe reduces significantly with increasing pressure.

First-principles band structure calculations were performed to rationalize the pressure induced semiconducting-semimetallic transition in SnSe. Plotted in Fig. 5a and b are the dispersion of energy bands and density of states of SnSe along the selected high

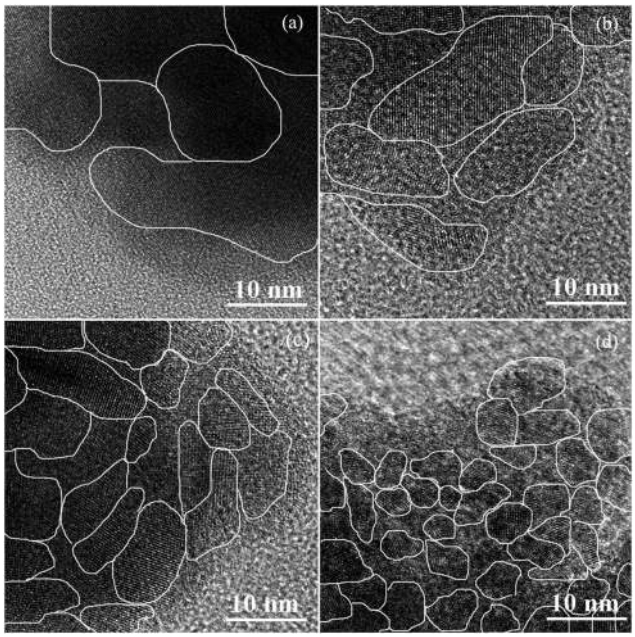

Fig. 4 High-resolution transmission electron microscopy images of SnSe quenched from different pressures: (a) ambient pressure, (b) 10 GPa, (c) 15 GPa and (d) 25 GPa, respectively.

symmetry points that are shown in Fig. 5c. It is found that, at zero pressure, SnSe is an indirect band gap semiconductor with the conduction band minimum (CBM) and the valence band maximum (VBM) located at the G point and along the G-Z line, respectively. The corresponding total and partial density of states (PDOS) are plotted in Fig. 5b. The Se-3s states are obviously separated from the other valence band states with a gap of 2.6 eV, showing strong lone electron pair character. The low-energy region from −8 to −5.1 eV consists of a large part of Sn-5s states coupled with Se-3p orbits. The moderate-energy region (−5.1 to −1.0 eV) is occupied by Sn-5p states strongly hybridized with Se-3p states. The high-energy region (−1.0 to 0 eV) is mainly made up of Sn-5s, Sn-5p, and S-3p combinations. Above the Fermi level, Sn-5p states and Se-3p states dominate the conduction bands of SnSe. Our results are consistent with previous calculations.[18]

Under compression, both the VBM and the CBM move toward the Fermi level gradually and subsequently the energy band gap is reduced. The band structures at 9 GPa (Fig. 5a red dotted lines) indicate that the conduction bands broaden significantly and traverse the Fermi energy level and overlap with valence bands, showing semimetallic character. By analyzing the PDOS at 9 GPa (Fig. 5b), the Sn-5s, Sn-5p, and Se-3p states are coupled significantly, which directly results in the closure of the band gap and thereby the transition from the semiconductor to semimetal in SnSe.

It is well-known that GGA-PBE systematically underestimates the energy band gap of the semiconductor.[38] Fortunately, the pressure dependence of the band gap was shown to be reliable.[39,40] In the case of SnSe, the band gap at zero pressure $E_g(0)$ is equal to

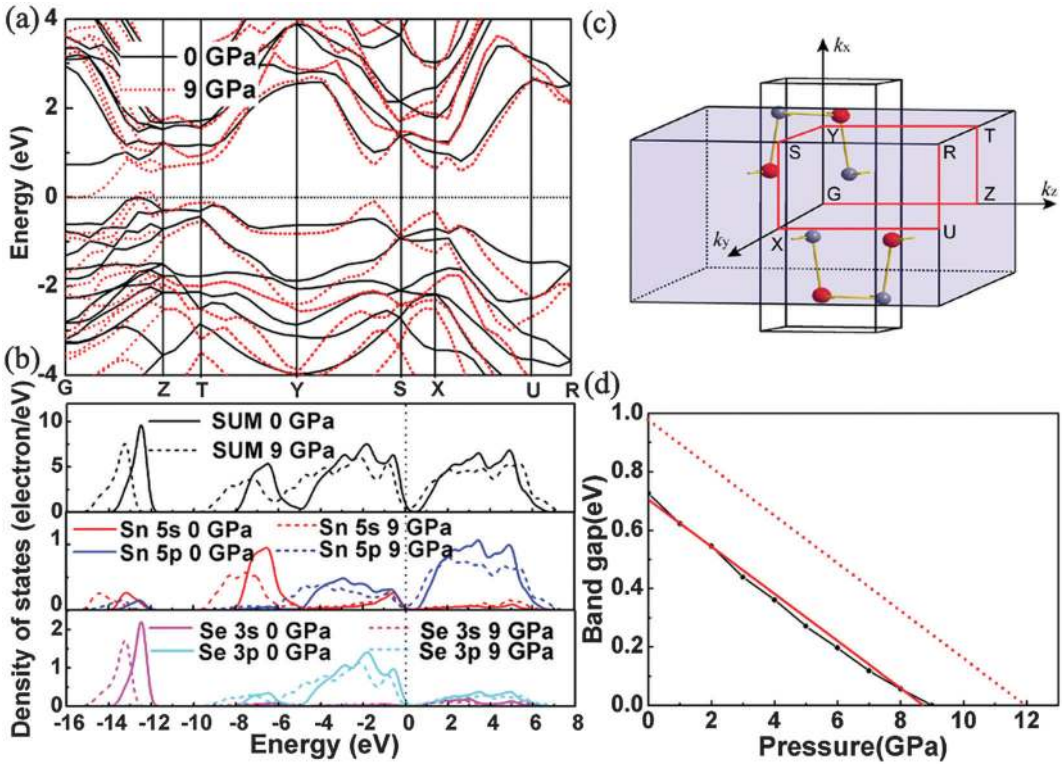

Fig. 5 (a) Band structure of SnSe along high-symmetry directions at 0 and 9 GPa. (b) The corresponding total and partial density of states at 0 GPa and 9 GPa. (c) The Brillouin zone of SnSe. (d) The energy band gap of SnSe as a function of pressure. The red dotted line is the E_g–P line after moving E_g (0) to 0.97 eV.

~0.73 eV, about ~19% lower than the previous experimental results.[41,42] By linear fitting the E_g *versus* P plots (Fig. 5d), we obtain the relationship of $E_g(P)$ and P:

$$E_g(P) = E_g(0) - 0.081P.$$

The experimental band gap of SnSe under ambient conditions is 0.89–1.05 eV.[41–44] We assume that the ambient-pressure band gap $E_g(0)$ is equal to their average values, 0.97 eV. If $E_g(P) = 0$, then P = 12 GPa, comparable with our temperature dependence of resistivity results. Besides, the non-hydrostatic conditions in electrical transport measurements may also slightly affect the transition pressure.[34,45,46]

The results in this study may be useful for optimizing the thermoelectric performance of SnSe. Applying compression can significantly modulate the electrical resistivity of SnSe by more than one order of magnitude. In addition, the pressure-induced nanostructuring on SnSe may enhance the scattering of phonons, and hence decrease lattice thermal conductivity κ_{lat}. All these factors should enhance ZT of SnSe under pressure.

4. Conclusions

In summary, we have studied the electrical transport and structural properties of SnSe under compression by using X-ray diffraction, temperature dependence of electrical resistivity, *in situ* Hall-effect measurements and first-principles calculations. SnSe transforms from a semiconducting to semimetallic state at 12.6 GPa, followed by an orthorhombic to monoclinic structural transition. Both the carrier concentration and mobility change are abnormally accompanied by the semiconducting-semimetallic transition. First-principles band structure calculations confirm the electronic transition, and reveal that the semimetal character of SnSe can be attributed to the enhanced coupling of Sn-5s, Sn-5p, and Se-3p states under compression, which results in the broadening of the energy bands and subsequent closure of the energy band gap. TEM images indicate that the average grain size of SnSe decreases significantly with increasing pressure. The pressure modulated variation of electrical transport and structural properties may provide an approach to improving the thermoelectric properties of SnSe.

Acknowledgements

This work was supported by the National Natural Science Foundation of China (Grant No. 11374121, and 11404133) and the Program of Science and Technology Development Plan of Jilin Province (Grant No. 20140520105JH).

References

1 A. Redinger, D. M. Berg, P. J. Dale and S. Siebentritt, *J. Am. Chem. Soc.*, 2011, **133**, 3320–3323.
2 E. Barrios-Salgado, M. T. S. Nair and P. K. Nair, *ECS J. Solid State Sci. Technol.*, 2014, **3**, 169–175.
3 M. A. Franzman, C. W. Schlenker, M. E. Thompson and R. L. Brutchey, *J. Am. Chem. Soc.*, 2010, **132**, 4060–4061.
4 M. Biçer and İ. Şişman, *Appl. Surf. Sci.*, 2011, **257**, 2944–2949.
5 Z. Zainal, S. Nagalingam, A. Kassim, M. Z. Hussein and W. M. M. Yunus, *Sol. Energy Mater. Sol. Cells*, 2004, **81**, 261–268.
6 L. D. Zhao, S. H. Lo, Y. Zhang, H. Sun, G. Tan, C. Uher, C. Wolverton, V. P. Dravid and M. G. Kanatzidis, *Nature*, 2014, **508**, 373–377.
7 J. P. Heremans, V. Jovovic, E. S. Toberer, A. Saramat, K. Kurosaki, A. Charoenphakdee, S. Yamanaka and G. J. Snyder, *Science*, 2008, **321**, 554–557.
8 L. D. Zhao, J. He, S. Hao, C. I. Wu, T. P. Hogan, C. Wolverton, V. P. Dravid and M. G. Kanatzidis, *J. Am. Chem. Soc.*, 2012, **134**, 16327–16336.
9 L. D. Zhao, G. J. Tan, S. Q. Hao, J. Q. He, Y. L. Pei, H. Chi, H. Wang, S. K. Gong, H. B. Xu, V. P. Dravid, C. Uher, G. J. Snyder, C. Wolverton and M. G. Kanatzidis, *Science*, 2016, **351**, 141–144.
10 L. D. Zhao, S. Hao, S. H. Lo, C. I. Wu, X. Zhou, Y. Lee, H. Li, K. Biswas, T. P. Hogan, C. Uher, C. Wolverton, V. P. Dravid and M. G. Kanatzidis, *J. Am. Chem. Soc.*, 2013, **135**, 7364–7370.
11 D. Errandonea, D. Martínez-García, A. Segura, J. Haines, E. Machado-Charry, E. Canadell, J. C. Chervin and A. Chevy, *Phys. Rev. B: Condens. Matter Mater. Phys.*, 2008, **77**, 045208.
12 D. Errandonea, D. Martínez-García, A. Segura, A. Chevy, G. Tobias, E. Canadell and P. Ordejon, *Phys. Rev. B: Condens. Matter Mater. Phys.*, 2006, **73**, 235202.
13 F. J. Manjón, D. Errandonea, A. Segura and V. Muñoz, *Phys. Rev. B: Condens. Matter Mater. Phys.*, 2001, **63**, 125330.
14 T. Chattopadhyay, A. Werner, H. G. von Schnering and J. Pannetier, *Rev. Phys. Appl.*, 1984, **19**, 807–813.
15 S. Alptekin, *J. Mol. Model.*, 2011, **17**, 2989–2994.
16 L. Ehm, K. Knorr, P. Dera, A. Krimmel, P. Bouvier and M. Mezouar, *J. Phys.: Condens. Matter*, 2004, **16**, 3545–3554.
17 I. Loa, R. J. Husband, R. A. Downie, S. R. Popuri and J-W. G. Bos, *Phys. Condens. Matter*, 2015, **27**, 072202.
18 L. Makinistian and E. A. Albanesi, *Comput. Mater. Sci.*, 2011, **50**, 2872–2879.
19 A. Agarwal, S. H. Chaki, S. G. Patel and D. Lakshminarayana, *J. Mater. Sci.: Mater. Electron.*, 1994, **5**, 287–290.
20 A. Agarwal, P. H. Trivedi and D. Lakshminarayana, *Cryst. Res. Technol.*, 2005, **40**, 789–790.
21 B. B. Nariya, A. K. Dasadia and A. R. Jani, *J. Optoelectron. Adv. Mater.*, 2013, **7**, 53–57.
22 M. Li, C. Gao, Y. Ma, D. Wang, Y. Li and J. Liu, *Appl. Phys. Lett.*, 2007, **90**, 113507.
23 F. Ke, J. Yang, C. L. Liu, Q. L. Wang, Y. Q. Li, J. K. Zhang, L. Wu, X. Zhang, Y. H. Han, B. J. Wu, Y. Z. Ma and C. X. Gao, *J. Phys. Chem. C*, 2013, **117**, 6033–6038.
24 C. X. Gao, Y. H. Han, Y. Z. Ma, A. White, H. W. Liu, J. F. Luo, M. Li, C. Y. He, A. M. Hao and X. W. Huang, *et al.*, *Rev. Sci. Instrum.*, 2005, **76**, 083912.
25 H. K. Mao, P. M. Bell, J. W. Shaner and D. J. Steinberg, *J. Appl. Phys.*, 1978, **49**, 3276–3283.

26 J. P. Perdew, K. Burke and M. Ernzerhof, *Phys. Rev. Lett.*, 1996, **77**, 3865–3868.
27 M. D. Segall, P. J. D. Lindan, M. J. Probert, C. J. Pickard, P. J. Hasnip, S. J. Clark and M. C. Payne, *J. Phys.: Condens. Matter*, 2002, **14**, 2717–2744.
28 A. C. Larson and R. B. Von Dreele, *General Structure Analysis System (GSAS) LAUR*, Los Alamos National Laboratory, New Mexico, 2004.
29 S. Asanabe and A. Okazaki, *Proc. Phys. Soc., London*, 1959, **73**, 824–827.
30 E. O. Kane, *The k-p Method, Semiconductors and Semimetals*, Academic, New York, 1966.
31 L. D. Dai, H. P. Li, H. Y. Hu and S. M. Shan, *J. Geophys. Res.*, 2008, **113**, 12211.
32 F. Ke, J. Yang, C. L. Liu, Q. L. Wang and Y. Q. Li, *et al.*, *J. Phys. Chem. C*, 2013, **117**, 6033–6038.
33 J. K. Zhang, C. L. Liu, X. Zhang, F. Ke, Y. H. Han, G. Peng, Y. Z. Ma and C. X. Gao, *Appl. Phys. Lett.*, 2013, **103**, 052102.
34 D. Errandonea, Y. Meng, M. Somayazula and D. Häusermann, *Physica B*, 2005, **355**, 116–125.
35 D. Errandonea, A. Segura, D. Martínez-García and V. Muñoz-San Jose, *Phys. Rev. B: Condens. Matter Mater. Phys.*, 2009, **79**, 125203.
36 H. Wiedemeier and H. G. von Schnering, *Z. Kristallogr.*, 1978, **148**, 295–303.
37 J. Zhang, H. Y. Zhu, X. X. Wu, H. Cui, D. M. Li, J. R. Jiang, C. X. Gao, Q. S. Wang and Q. L. Cui, *Nanoscale*, 2015, **7**, 10807–10816.
38 J. Ruiz-Fuertes, S. López-Moreno, J. López-Solano, D. Errandonea, A. Segura, R. Lacomba-Perales, A. Muñoz, S. Radescu, P. Rodríguez-Hernández, M. Gospodinov, L. L. Nagornaya and Y. C. Tu, *Phys. Rev. B: Condens. Matter Mater. Phys.*, 2012, **86**, 125202.
39 C. J. Wu, L. H. Yang, L. E. Fried, J. Quenneville and T. J. Martinez, *Phys. Rev. B: Condens. Matter Mater. Phys.*, 2003, **67**, 235101.
40 V. Fiorentini, *Phys. Rev. B: Condens. Matter Mater. Phys.*, 1992, **46**, 2086–2091.
41 M. Parenteau and C. Carlone, *Phys. Rev. B: Condens. Matter Mater. Phys.*, 1990, **41**, 5227–5234.
42 H. S. Soliman, D. A. Abdel Hady, K. F. Abdel Rahman, S. B. Youssef and A. A. E1-Shazly, *Physica A*, 1995, **216**, 77–84.
43 A. M. Elkorashy, *J. Phys. Chem. Solids*, 1986, **47**, 497–504.
44 B. Subramanian, T. Mahalingam, C. Sanjeeviraja, M. Jayachandran and M. J. Chockalingam, *Thin Solid Films*, 1999, **357**, 119–124.
45 S. Klotz, J. C. Chervin, P. Munsch and G. L. Marchand, *J. Phys. D: Appl. Phys.*, 2009, **42**, 075413.
46 D. Errandonea, A. Muñoz and J. Gonzalez-Platas, *J. Appl. Phys.*, 2014, **115**, 216101.

